

Lindblad parameters from high resolution spectroscopy to describe collision induced decoherence in the gas phase – Application to acetylene

Antoine Aerts,¹ Jean Vander Auwera,¹ and Nathalie Vaeck^{1, a)}

Université Libre de Bruxelles; Spectroscopy, Quantum Chemistry and Atmospheric Remote Sensing (SQUARES); 50 avenue F. Roosevelt, C.P. 160/09, B-1050 Brussels, Belgium

(Dated: 21 March 2022)

Within the framework of the Lindblad master equation, we propose a general methodology to describe the effects of the environment on a system in dilute gas phase. The phenomenological parameters characterizing the transitions between rovibrational states of the system induced by collisions can be extracted from experimental transition kinetic constants, relying on Energy Gap fitting laws. As the availability of this kind of experimental data can be limited, the present work relied on experimental line broadening coefficients, however still using Energy Gap fitting laws. The 3 μm infrared spectral range of acetylene was chosen to illustrate the proposed approach. The method shows fair agreement with available experimental data while being computationally inexpensive. The results are discussed in the context of state laser quantum control.

^{a)}Email: nvaeck@ulb.ac.be

CREDIT

The following article has been submitted to The Journal of Chemical Physics.

I. INTRODUCTION

With the increasing availability of computational power and promises of the quantum technologies, the impact of decoherence processes caused by the interactions with the environment is receiving more and more attention in studies of the dynamics of realistic open systems.¹ It is worth to mention the importance of decoherence in the context of molecular rotation² control, which is particularly relevant in this case, but also in biological systems,³ charge transfer in molecules,⁴ vibration of adsorbed molecules⁵ or chemical reactions.⁶ In the context of quantum control, decoherence caused by the interaction of the system of interest with its environment is a major issue for applications. Decoherence can act against the control performance or induce a loss of “quantum” property (loss of coherence). In spite of this, theoretical control studies were mainly conducted in the gas phase without assessment of environment-induced processes.

The primary source of decoherence, inherent to the system, arises from intramolecular vibrational redistribution (IVR) and was discussed before.⁷ It is included in the simulation dynamics by design.^{7,8} All environmental effects acting on the molecule are expected to cause decoherence that, in the gas phase, is well pictured by the alteration of the shape of the spectral lines.⁹ It can easily be shown that collisions are the main source of shape alteration at atmospheric pressure, giving rise in the time domain to population transfers from one rotational level to another.

Rotational decoherence is particularly important in the understanding of dissipation occurring in gases. Its effects can be studied by a variety of experimental techniques including infrared-ultraviolet double resonance (IRUVDR)¹⁰ or molecular centrifuges more suitable for studies of high angular momenta.^{11,12} The rotational relaxation can also be computed *ab initio*,¹³ however requiring a significant computational effort to obtain the intermolecular potential and to calculate the *S*-matrix. An alternative method involves the study of lineshapes in the spectral domain. Collision-induced decays or transfers of rotational populations indeed condition the shape of spectral lines, as modeled by the relaxation matrix.^{14,15}

The elements of this matrix can be measured experimentally or calculated. In particular, the real part of the relaxation matrix can be constructed in a rather simple way using Energy Gap fitting laws.¹⁵ Energy Gap fitting laws arise from the intuitive picture that rotational relaxation should drop with the change of rotational quantum number J , or equivalently with the energy difference, induced by the collisions. This intuitive picture was well reproduced in experimental studies since its first mention,¹⁶ and has spawned the development of numerous energy based scaling laws,¹⁷ which for example proved to be successful in the description of line mixing effects in collisionally-broadened CO₂ infrared branches.¹⁸⁻²⁰

The aim of the present work is to couple high resolution spectroscopy with quantum dynamics in the context of collision dynamics in the gas phase. High resolution spectroscopic data on acetylene (effectively its main isotopologue ¹²C₂H₂) were used to illustrate the purpose. The time evolution induced by collisions of the population of a rovibrationally excited level of acetylene in a dilute gas phase is calculated using the Lindblad master equation, the required (Lindblad) parameters being obtained from either pump-probe experiments or collisional line broadening coefficients, relying on Energy Gap fitting laws. Approaches used in this work are well established in their respective communities; this article tries to present them in an unified manner. The present work is part of our effort to better understand the dynamics and the control of the vibrational population of acetylene to possibly access the vinylidene isomer. It was shown that a specific vibrational mode of acetylene (C₂H₂) in dilute gas phase can be populated using a single shaped laser pulse.⁷ In other words, a state well isolated from others with respect to IVR could be specifically populated via the control of the population of vibrational levels of C₂H₂. This study was later⁸ extended by inclusion of the rotational structure in the description of the controlled system state, which proved to be essential for the determination of the control pulse shape. Another important aspect of the proposed protocol is to establish a methodology to allow taking into account the effect of the environment, which is the purpose of this work.

In the next sections, the vibration-rotation structure of the acetylene molecule is briefly introduced followed by the Lindblad master equation that describes the quantum dynamics in a system, including the effects of its environment. The determination of the Lindblad parameters from pump probe experiments and collisional line broadening coefficients is then detailed. This article concludes with some perspectives.

II. THE VIBRATION-ROTATION STRUCTURE OF ACETYLENE

The vibrational motion of the main isotopologue of the acetylene molecule, $^{12}\text{C}_2\text{H}_2$, can be described in terms of the 5 modes of vibration presented in Table I. The zero-order vibrational levels associated with the excitation of these modes are identified by $|v_1 v_2 v_3 v_4^{\ell_4} v_5^{\ell_5}\rangle$, where v_i is the vibrational quantum number associated with the mode of vibration ν_i ($i = 1 \dots 5$, see Table I) and ℓ_4 and ℓ_5 are the quantum numbers associated with the vibrational angular momenta generated by the excitation of the doubly degenerate bending modes ν_4 and ν_5 , respectively. These vibrational levels interact mostly through anharmonic resonances, leading to the formation of so-called polyads.²¹

The present work focuses on the polyad of vibrational levels of the ground electronic state of $^{12}\text{C}_2\text{H}_2$ that gives rise to the strong $3 \mu\text{m}$ infrared absorption of this molecule when accessed from the vibrational ground state. This polyad involves 3 zero-order levels, namely $|0010^00^0\rangle$, $|0101^11^{-1}\rangle$ and $|0101^11^1\rangle$. Allowed one-photon transitions from the ground state only involve the $|0010^00^0\rangle$ level. It is therefore identified as a “bright” level, while the other two are identified as “dark” levels. Anharmonic resonances strongly mix the $|0010^00^0\rangle$ and $|0101^11^{-1}\rangle$ levels, while the $|0101^11^1\rangle$ level essentially keeps its “dark” character.^{7,22} As this latter level was shown to not being involved in the collisional processes considered here,^{23,24} it will not be considered any further. The eigenstates resulting from the mixing of the former two levels are identified from now on as Γ_1 and Γ_2 , Γ_2 having the highest energy of the two. Transitions from the ground state to Γ_1 and Γ_2 result into two strong bands observed near $3 \mu\text{m}$, which are called experimentally the $\nu_2 + (\nu_4 + \nu_5)_+^0$ and ν_3 bands, respectively. The exponent 0 appearing for the former band is the value of $k = \ell_4 + \ell_5$ and the “+” sign refers to the symmetry of the vibrational wavefunction with respect to the infinity of planes containing the molecule.²⁵

In section V, self broadening coefficients of vibration-rotation lines of the ν_3 band are needed. However, they have never been directly measured for this band, most probably because of its strength. Fortunately, the vibrational dependence of self broadening coefficients is generally small and has never clearly been evidenced for acetylene.²⁶ In the frame of the present work, we therefore relied on the extensive set of self broadening coefficients measured for the $3\nu_5^1$, $(2\nu_4 + \nu_5)^1\text{I}$ and $(2\nu_4 + \nu_5)^1\text{II}$ bands observed in the $5 \mu\text{m}$ region ($1860 - 2180 \text{ cm}^{-1}$).²⁶ The Roman numerals I and II discriminate the two $k = 1$ vibrational

Normal mode	$\text{H}—\text{C}\equiv\text{C}—\text{H}$	Harmonic frequency / cm^{-1}
ν_1		3389.12
ν_2		1950.11
ν_3		3310.02
ν_4		604.47
ν_5		728.27

TABLE I. Normal modes of vibration of acetylene $^{12}\text{C}_2\text{H}_2$ in its ground electronic state and their harmonic frequencies.²⁹ The first three are non degenerate stretching modes and the last two are doubly degenerate bending modes.

levels with the same symmetry that arise from the simultaneous excitation of 2 quanta in ν_4 and one quantum in ν_5 , the Roman numeral I identifying the level characterized by the highest energy.^{27,28}

Acetylene is a linear molecule in its ground electronic state. Therefore, the description of its rotational motion mainly involves the quantum number J associated with the angular momentum of the molecule.

III. LINDBLAD EQUATION

The evolution of a system coupled to the environment in the Born and Markov approximation can be described by the Lindblad master equation:^{30,31}

$$\begin{aligned} \frac{d\hat{\rho}(t)}{dt} = & -\frac{i}{\hbar} \left[\hat{H}(t), \hat{\rho}(t) \right] \\ & + \sum_{ij} \left(\hat{L}_{ij} \hat{\rho}(t) \hat{L}_{ij}^\dagger - \frac{1}{2} \left[\hat{\rho}(t), \hat{L}_{ij}^\dagger \hat{L}_{ij} \right]_+ \right) \end{aligned} \quad (1)$$

where $\hat{H}(t) = \hat{H}_S - \hat{\mu}^e \epsilon(t)$ is the total Hamiltonian in the absence of interaction with the environment and \hat{H}_S the Hamiltonian of the system. If a laser field is applied, $\hat{\mu}^e$ is the electric dipole moment of the system and $\epsilon(t)$ is the time-dependent amplitude of the laser pulse. $[A, B]_+$ is the anti-commutator of arguments A and B , $\hat{\rho}(t)$ is the time-dependent density operator and \hat{L}_{ij} are operators representing the transitions induced by

the environment between states i and j of the system. A phenomenological representation of the transition operator was used:

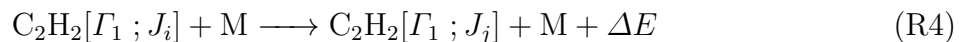
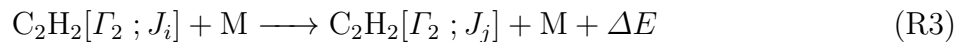
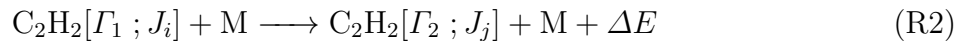
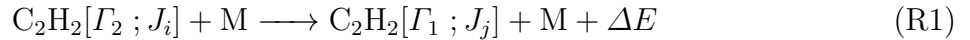
$$\hat{L}_{ij} = \sqrt{\theta_{ij}}|i\rangle\langle j|. \quad (2)$$

With this form, decoherence in the system is characterised by the Lindblad parameters θ_{ij} , which are the frequencies of the transitions induced by non-radiative processes¹ between eigenstates $|i\rangle$ and $|j\rangle$ of the system Hamiltonian. Comments on the implementation of the Lindblad master equation are given in the Supplemental Material. The determination of the Lindblad parameters θ_{ij} from experimental data published in the literature is discussed in the next two sections.

IV. LINDBLAD PARAMETERS FROM PUMP-PROBE EXPERIMENTS

Frost²³ and Henton *et al.*²⁴ studied experimentally the dynamical effects of collisions in the Γ_1 and Γ_2 interacting states using infrared ultraviolet double resonance (IRUVDR). An infrared “pump” laser of fixed wavelength was used to populate a specific rotational level of the eigenstate Γ_1 or Γ_2 and an ultraviolet “probe” laser induced a transition from the excited rovibrational level to the first excited electronic state. Collision-induced transitions within the eigenstates Γ_1 and Γ_2 were monitored from the observed evolution of the laser induced fluorescence with the probe laser wavelength. The corresponding state-to-state rate constants for rotational relaxation were determined. Frost²³ initiated the study for self-relaxation (C_2H_2 in an environment of C_2H_2), while Henton *et al.*²⁴ refined his measurements and extended this research to the effects of foreign gases (Ar, He and H_2) on the dynamics.

Frost²³ and Henton *et al.*²⁴ considered four relaxation processes caused by collisions. They are described as follows :



¹ The use of θ is a deliberate choice; γ is generally used in the literature.

where M is the collision partner (*i.e.* other C_2H_2 molecules in the present case), J_i and J_j are respectively the initial and final rotational levels and ΔE is the energy released/absorbed during the collision. It is worth noting that these processes are subject to the parity selection rule³² that forbids the change of the total wavefunction parity,³³ *i.e.* ortho \leftrightarrow para transitions are not observed.^{23,24} Ortho and para label the levels with the highest and lowest nuclear spin statistical weights, respectively. In $^{12}C_2H_2$, ortho (*resp.* para) labels levels with odd (*resp.* even) J . Consequently, non-radiative transitions involving even $\Delta J = |J_j - J_i|$ are solely observed in experiments.

Frost²³ and later Henton *et al.*²⁴ determined the transition kinetic constants $k(j \leftarrow i)$ of processes R1 to R4 using the IRUVDR technique. They fitted their measurements to Exponential Gap Laws (EGL) of the form:

$$k(j \leftarrow i | K_0, \eta) = K_0 \exp\left(\frac{-\eta|E_j - E_i|}{k_B T}\right) \quad \text{with } E_j > E_i \quad (3)$$

where K_0 (in units of frequency per pressure as k) and η (dimensionless) are fitted parameters and E_i is the energy of level i . Their reported parameters and uncertainties are reproduced in Table II, together with the identification of the level populated by the pump laser. Table II shows that the η parameters of the 5 different processes have the same value within the stated uncertainties. On the other hand, comparisons of the magnitude of the K_0 parameters show that transitions within the same vibrational eigenstate (R3 and R4) are an order of magnitude faster than transitions involving a change of eigenstate (R1 and R2) and that transitions with $\Delta J = \pm 2$ in the Γ_1 eigenstate are greatly favoured. In this later case, the η parameter was fixed by Henton *et al.*²⁴ to the value reported for the $\Delta J \geq 4$ transitions, given the expected strong correlation of the parameters.³⁴

To express the Lindblad parameters θ_{ij} (see Eq. 2) from this data set, we assumed that they are related to the transition kinetic constants $k(j \leftarrow i)$ by:

$$\theta_{ij} = P k(j \leftarrow i) \quad (4)$$

The linear dependence with pressure should be suitable for P up to 1 atm.³⁵ A correction to the collision frequency may however be needed at higher pressure,³⁶ or even a different approach,³⁷ because the IRUVDR measurements could not be extrapolated to that regime and equations given in the present work would not hold.

The experimental results and the choice of the EGL somewhat validate the Lindblad master equation in this case as the decays induced by the master equation are exponential.³⁸

Process	K_0	η	Initial
R1	0.005(1)	1.7(7)	$\Gamma_2, J = 12$
R2	0.0036(3)	0.91(31)	$\Gamma_1, J = 10$
R3	0.032(3)	1.92(17)	$\Gamma_2, J = 12$
R4, $ \Delta J = 2$	0.045(7)	1.71	$\Gamma_1, J = 10$
R4, $ \Delta J \geq 4$	0.019(3)	1.71(27)	$\Gamma_1, J = 10$

TABLE II. Experimental parameters (K_0 in $\text{cm}^{-1}\text{atm}^{-1}$ and η is dimensionless) of the EGL law (Eq. 3) from Frost²³ and Henton *et al.*²⁴ used in this work to calculate the kinetic constants of processes R1 to R4. Numbers between parentheses are the standard deviations in the units of the last digit quoted. The last column identifies the level initially populated by the pump laser.

It can indeed be shown that, for an eigenstates system dynamics driven solely by interaction with its environment $\left(-\frac{i}{\hbar} [\hat{H}(t), \hat{\rho}(t)] = 0\right)$, Eq. 1 simplifies to a sum of products of scalars and density matrices when the phenomenological representation of the transition operators is used (see Eqs. S3 and S4 in the Supplemental Material).

To illustrate the collision-induced dynamics, Fig. 1 shows the evolution of the relative population of selected levels of the polyad of interest at $P = 1$ atm, as described by the Lindblad master equation (Eq. 1) without interaction with an external laser field. The transitions frequencies θ_{ij} are obtained from Eqs. 4 and 3, and the experimental EGL parameters given in Table II. The H_S hamiltonian of acetylene itself is described in the state space by a global effective hamiltonian,²¹ built from the extensive set of experimental high-resolution spectroscopic studies carried out in the ground electronic state of the molecule. More details can be found in our previous work,^{7,8} and a thorough and pedagogical introduction to the strategy applied to build such global hamiltonians was given by Herman.³⁹ Working in the state space connects the relevant quantities obtained from high resolution spectroscopy, *i.e.* eigenstates energies from line positions and transition dipole moment operators from line intensities, to the system dynamics. The state basis used for the simulation includes levels from $J=0$ to $J=100$. The initial population lies in the $\Gamma_2, J = 12$ rovibrational level as an illustration of the dynamics probed by the experiments of Frost.²³ The dynamics is solely driven by population transfers between rotational levels induced by inelastic collisions, *i.e*

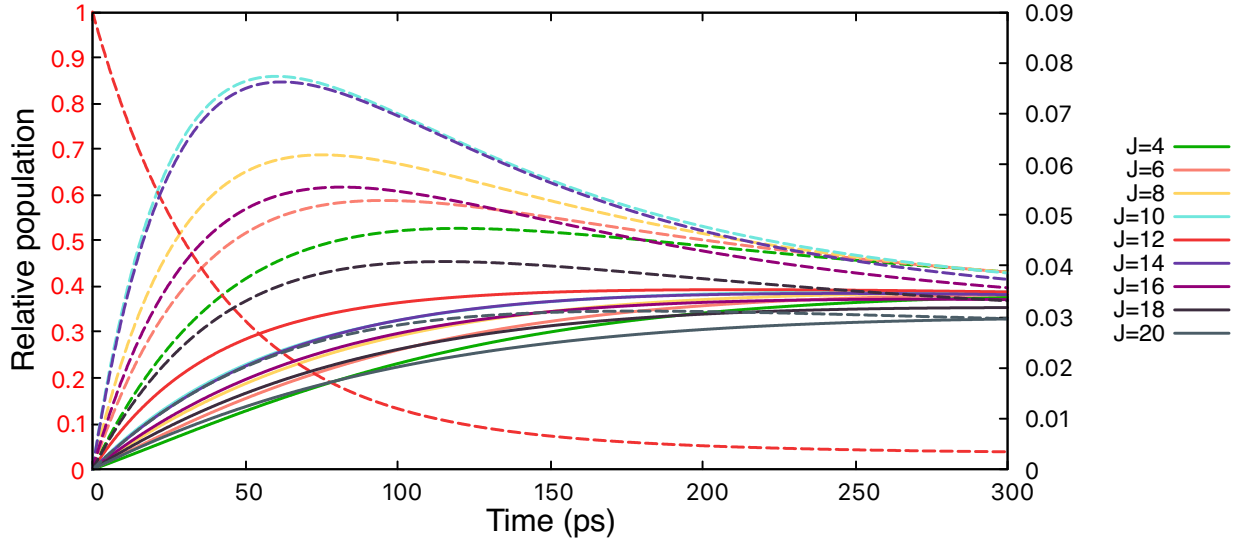


FIG. 1. Collision induced dynamics in Γ_1 (**continuous**) and in Γ_2 (**dashed**) from unitary population in the $\Gamma_2, J = 12$ state (shown in red and on the right axis) under $P = 1$ atm. State-to-state transition frequencies are calculated from Eqs. 4 and 3, and the parameters reported by Frost²³ and Henton *et al.*²⁴ (reproduced in Table II).

transfers from/to another polyad or vibrational level are neglected as are parity-violating transitions that happen on a longer timescale. The simulation shows a rapid population transfer from the initially populated state to other states (almost complete within 100 ps), with a larger propensity for transfers within the same vibrational eigenstate. The statistical limit is almost reached within a few hundreds of ps. This means that any successful state-control targeting either the Γ_1 or Γ_2 eigenstates or any combination would therefore rapidly (*i.e.* within hundreds of ps) be lost due to collision-induced transitions.

V. LINDBLAD PARAMETERS FROM LINE BROADENING COEFFICIENTS

As detailed in the previous section, the Lindblad parameters θ_{ij} required to model population transfers induced by collisions between molecules in the gas phase in laser and environment-driven dynamics simulations can be taken from direct kinetic measurements. However, this kind of experimental data may not be available. In this section, we describe the alternative methodology we used to determine the parameters of the EGL law, namely K_0 and η , from self broadening coefficients.

In this perspective, we opt for the impact and binary collision approximations, relying on the construction of the real part of the relaxation matrix and statistically based on Energy Gap fitting laws.^{15,40} The approximations imply that the resulting perturbation on the spectrum is proportional to the gas density (binary collisions) and that the duration of the collisions is negligibly short, so that the perturbation is independent of the frequency over the spectral range considered (impact approximation).

Using the relaxation matrix (W) and including the relevant factors for intensities, the absorption coefficient α (in cm^{-1}) is given by the imaginary part of the (unnormalised) line profile:^{15,40}

$$\begin{aligned} \alpha(\tilde{\nu}, P, T) &= \frac{8\pi^3}{3hc} \frac{1}{4\pi\epsilon_0} \frac{n_L T_0}{Q(T)T} [1 - \exp\{-hc\tilde{\nu}/k_B T\}] \tilde{\nu} \\ &\times \frac{1}{\pi} \sum_{\ell} \sum_{\ell'} \rho_{\ell}(T) d_{\ell} d_{\ell'} \{[\Sigma - L_a - iPW(T)]^{-1}\}_{\ell' \ell} \end{aligned} \quad (5)$$

where $8\pi^3/(3hc)(1/(4\pi\epsilon_0)) \approx 4.16237 \times 10^{-19} \text{ D}^{-2} \text{cm}^2$, $n_L = 2.686780111 \times 10^{19} \text{ cm}^{-3} \text{atm}^{-1}$ is the Loschmidt constant, $T_0 = 273.15 \text{ K}$ and $Q(T)$ is the total internal partition sum with $Q(^{12}\text{C}_2\text{H}_2) = 412.45$ at 296 K ,⁴¹ $\tilde{\nu}$ is the wavenumber (in cm^{-1}), P is the pressure of the perturber (in atm), T is the temperature (in K), $\rho_{\ell}(T)$ is the equilibrium relative population of the initial level of line ℓ , d_{ℓ} is the tensor that couples radiation and matter (electric dipole moment in this case, in Debye) for line ℓ and i is the imaginary number. Σ and L_a are defined in the line space as:

$$\Sigma_{\ell' \ell} = \delta_{\ell, \ell'} \times \tilde{\nu} \quad (6)$$

$$\{L_a\}_{\ell' \ell} = \delta_{\ell, \ell'} \times \tilde{\nu}_{\ell} \quad (7)$$

with $\tilde{\nu}_\ell$ the position of line ℓ and $\delta_{\ell,\ell'} = \delta_{i_\ell,i_{\ell'}} \delta_{f_\ell,f_{\ell'}}$ where i_ℓ and f_ℓ are the initial and final rotational or rotation-vibration levels of the transition associated with line ℓ . Both are diagonal matrices of size $N \times N$ in the line space, where N is the number of lines.

The photon interacting with the molecules undergoing collisions is eventually dissipated in the system with a resulting broadening and shifting of the resonance wavenumber. This is modeled using the relaxation matrix W , which adds a complex perturbation to the resonance wavenumber within the impact approximation. The relaxation matrix is constructed with line broadening (real part) and line shift (imaginary parts) coefficients on its diagonal. The real part of the non-diagonal elements model line mixing effects on the line shape, their imaginary part being usually small and neglected.^{15,42} Only considering the diagonal elements of W , the spectrum calculated with Eq. 5 is a sum of Lorentzian. The term $[\Sigma - L_a - iPW(T)]$ is a complex matrix of size $N \times N$ (N is the number of lines), which must be inverted. Details on how to simulate a spectrum using Eq. 5 along with an illustration for the ν_3 band of $^{12}\text{C}_2\text{H}_2$ are provided in the Supplemental Material.

As demonstrated by Fano,⁴³ the line broadening coefficients γ_ℓ (at half width at half maximum, HWHM) of the (spectral) line ℓ are related to the state-to-state kinetic constants k by:

$$\text{Re}[W_{\ell\ell}] = \gamma_\ell = \frac{1}{2} \left\{ \sum_{i_{\ell'} \neq i_\ell} k(i_{\ell'} \leftarrow i_\ell) + \sum_{f_{\ell'} \neq f_\ell} k(f_{\ell'} \leftarrow f_\ell) \right\}. \quad (8)$$

The first sum describes collision-induced transitions between rotational levels in the lower vibrational level (for cold bands, i_ℓ levels belong to the ground vibrational state) and the second sum describes collision-induced transitions in the excited vibrational level(s). Both contributions are often assumed to be of similar magnitude. Again, the kinetic constants k can be parametrized using a number of “gap” laws. One of the simplest is the Exponential Gap Law (EGL) (Eq. 3). Alternatively, a third parameter can be introduced using the Exponential Power Gap Law (EPGL) given by:

$$k(j \leftarrow i | K_0, \eta, \beta) = K_0 \left(\frac{|E_j - E_i|}{k_B T} \right)^{-\beta} \exp \left(\frac{-\eta |E_j - E_i|}{k_B T} \right) \quad \text{with } E_j > E_i \quad (9)$$

where K_0 (same units as k), β and η are the fitted parameters and E_i is the energy of level i . The downwards transition kinetic constants are deduced from Eq. 3 (or 9) and the detailed

balance (to ensure conservation of total population):

$$k(i \leftarrow j) = \frac{\rho_i}{\rho_j} k(j \leftarrow i) = \frac{2J_i + 1}{2J_j + 1} \exp\left(\frac{E_j - E_i}{k_B T}\right) k(j \leftarrow i) \quad (10)$$

with ρ_i the relative population of level i , proportional to $(2J_i + 1) \exp(-E_i/k_B T)$.

The interacting system $\Gamma_1 - \Gamma_2$ considered here requires some care as it may not be as straightforward to calculate the broadening coefficients from the state-to-state kinetic constants using Eq. 8 as it may seem. The last term of the right part of Eq. 8 must indeed include the relevant transfer channels in the excited vibrational levels described by reactions R1 to R4, *e.g.* R1 and R3 for the Γ_2 eigenstate. In addition, the selection rule that forbids parity change of J in collision-induced transitions must be taken into account:

$$\sum_{f_{\ell'} \neq f_{\ell}} k(f_{\ell'} \leftarrow f_{\ell}) = \sum_{c=1}^{N_c} \sum_{f_{\ell'} \neq f_{\ell}} k_c(f_{\ell'} \leftarrow f_{\ell}) \quad (11)$$

$$\Delta J = J_{f_{\ell'}} - J_{f_{\ell}} = \text{even}$$

where k_c is the state-to-state kinetic constant within channel c and N_c is the number of channels ($N_c = 2$ for each vibrational eigenstate here; see Eqs. 13 and 14 for the explicit sums).

Broadening coefficients have never been directly measured for the ν_3 band of acetylene, most probably because of the large transition dipole moment associated with this band. However, vibrational dependence of the broadening coefficients (HWHM) is generally small, especially in acetylene.²⁶ Therefore, we used the extensive set of experimental broadening coefficients measured for cold bands in the 5 μm region of acetylene.²⁶ They are presented in Fig. 2. The error bars associated with these data correspond to the upper limit of their reported precision of measurement,⁴⁴ *i.e.* 5 %.

The broadening coefficients predicted using the EGL parameters of Frost²³ and Henton *et al.*²⁴ (see Table II) are also presented in Fig. 2. They were calculated using Eq. 8 restricted to non radiative transitions within the excited vibrational level, *i.e.*

$$\gamma_{\ell} = \sum_{f_{\ell'} \neq f_{\ell}} k(f_{\ell'} \leftarrow f_{\ell}), \quad (12)$$

due to the lack of measurements reported for the ground vibrational state, together with Eqs. 3, 10 and 11. The labels Γ_1 and Γ_2 in Fig. 2 identify the nature of the excited vibrational level. The energies of the vibrational eigenstates of interest were calculated

using the effective Hamiltonian,²¹ with rotational quantum number up to $J = 100$. Energies agree with reported experimental line positions^{22,45} with a root mean square deviation of 0.0007 cm⁻¹.

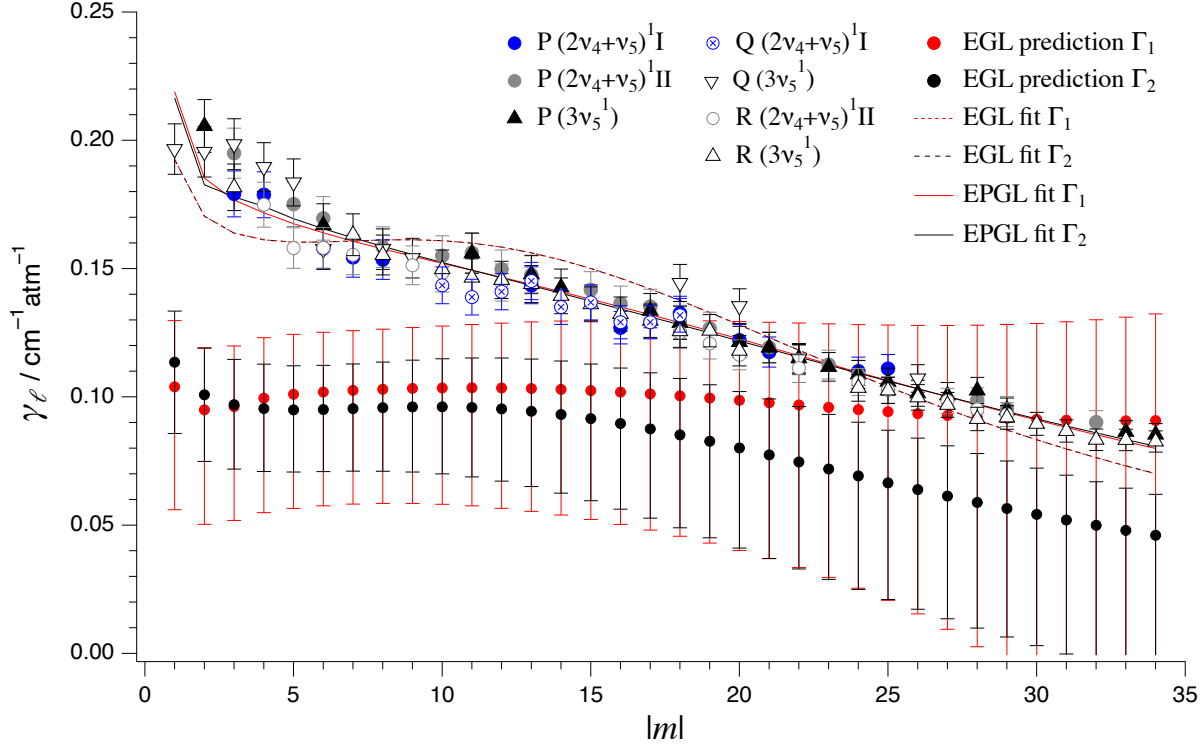


FIG. 2. Dependence of line broadening coefficients γ_ℓ (HWHM) with the absolute value of the rotational quantum number ($|m| = J_i + 1$ for R branch lines and $|m| = J_i$ for P and Q branch lines). The experimental data measured for cold bands in the 5 μm region of acetylene²⁶ are compared with values predicted and fitted using the EGL and EPGL (see text for details). The lines are guides for the eyes.

Fig. 2 shows that the predictions underestimate the broadening coefficients of most lines suggesting that elastic collisions, not considered by Frost²³ and Henton *et al.*,²⁴ contribute significantly to line broadening. Additionally, the predicted rotational dependence does not match the observation, probably because it involves extrapolation of an undersized set of measurements (only from one J to others).

In view of these disagreements, the values of the parameters K_0 and η involved in the EGL modeling of the transition kinetic constants $k(j \leftarrow i)$ were determined by fitting Eqs. 3 and 10 to 12 to the measured broadening coefficients²⁶ presented in Fig. 2. Additionally, Eq. 11

was adapted in two ways. Orr suggested⁴⁶ that the contributions of processes such as R1 and R2 should correspond to at most 10% of the total transition frequency from one rotational level. In Eq. 11, the sum of state-to-state transition frequencies of processes R1 and R2 was therefore constrained to contribute to 10% of the broadening coefficient (processes R3 and R4 thus contribute to 90%). Although the contributions of R1 and R2 were later refined to approximately 21% in the polyad of interest using direct measurements of state-to-state kinetic constants,^{24,47} confirming Orr’s suggestion that the intramolecular couplings enhance vibration – vibration transfers,⁴⁶ significant uncertainties remain. To highlight the ability of the present methodology to describe the environment-induced processes in generic problems, this work relied on as few specific parameters as possible; this refined measurement was therefore ignored. Additionally, to keep the problem tractable and avoid strong correlations between parameters, the number of fitted parameters was restricted to two sets identified by the upper level of the transition belonging to either the Γ_1 (R2 and R4) or Γ_2 (R1 and R3) eigenstate. Taking these two constraints into account, Eqs. 12 and 11 become in the EGL:

$$\gamma_{\ell}^{\Gamma_1} = 0.1 \sum_{f_{\ell'} \neq f_{\ell}} k_{R2}(f_{\ell'}^{\Gamma_2} \leftarrow f_{\ell}^{\Gamma_1} | K_0^{\Gamma_1}, \eta^{\Gamma_1}) + 0.9 \sum_{f_{\ell'} \neq f_{\ell}} k_{R4}(f_{\ell'}^{\Gamma_1} \leftarrow f_{\ell}^{\Gamma_1} | K_0^{\Gamma_1}, \eta^{\Gamma_1}) \quad (13)$$

$$\gamma_{\ell}^{\Gamma_2} = 0.1 \sum_{f_{\ell'} \neq f_{\ell}} k_{R1}(f_{\ell'}^{\Gamma_1} \leftarrow f_{\ell}^{\Gamma_2} | K_0^{\Gamma_2}, \eta^{\Gamma_2}) + 0.9 \sum_{f_{\ell'} \neq f_{\ell}} k_{R3}(f_{\ell'}^{\Gamma_2} \leftarrow f_{\ell}^{\Gamma_2} | K_0^{\Gamma_2}, \eta^{\Gamma_2}) \quad (14)$$

where the transition kinetic constants are given by Eq. 3. All broadening coefficients reported by Jacquemart *et al.*²⁶ for cold bands in the 5 μm region of acetylene were included in the fitting procedure. The coefficients reported for the same value of $|m|$ were averaged and assigned to transitions independently of their upper level belonging to the Γ_1 or Γ_2 eigenstate. The fitting was performed using the optimization library of SciPy⁴⁸ (scipy.optimize) with all tolerance parameters set to machine epsilon. The best-fit values of the EGL parameters obtained are given in Table III and the corresponding rotational dependences of the broadening coefficients are presented in Fig. 2 (dashed lines identified by “EGL fit Γ_1 ” and “EGL fit Γ_2 ,” actually overlapped). Fig. 2 shows that, although the EGL reproduces the general decrease of the broadening coefficients with increasing rotation, it exhibits additional oscillations. It is worth to point out that the EGL cannot adequately reflect the effects of the energy differences as all parameters are the same except for the proportionality weights of 10 and 90 % imposed to the contributions of processes R1 and R3 (for Γ_2) and R2 and

	K_0	η	β
EGL			
Γ_1	0.064(2)	1.98(5)	/
Γ_2	0.064(2)	1.98(5)	/
EPGL			
Γ_1	0.034(2)	1.43(5)	0.35(3)
Γ_2	0.032(2)	1.37(5)	0.37(3)

TABLE III. Best-fit values of the parameters of the two Energy Gap fitting laws used in this work (see text for details). K_0 are in $\text{cm}^{-1}\text{atm}^{-1}$; the other parameters are unitless. Γ_1 and Γ_2 identify the eigenstates of the upper level of the transition (appearing as an exponent in Eqs. 13 and 14). The numbers between parentheses are the standard deviations in the units of the last digit quoted.

R4 (for Γ_1) (Eqs. 13 and 14). As the EGL parameters of Frost²³ and Henton *et al.*²⁴ yield broadening coefficients smaller than observed, it is not surprising that the present fit results in larger values of the K_0 and η parameters. The fitted exponential parameters (η) however lie within the uncertainties of most reported ones (see Table II).

As shown in Fig. 2, the introduction of an additional parameter β in the EPGL (Eq. 9) results in a better description of the rotational dependence of the broadening coefficients. The resulting best-fit values of the parameters of the EPGL are also presented in Table III.

Fig. 3 shows a simulation of population dynamics for selected states in the polyad of interest, similar to those presented in Fig. 1. The Lindblad parameters are calculated using both the EPGL approach and its parameters listed in Table III and the EGL with its parameters listed in Table II. The state basis used for the simulation is the same as for Fig. 1. Note that our fitting procedure within the impact and binary collision approximations includes level energies up to $J=100$ and broadening coefficients up to $|m|=34$ while IRU-VDR measurements^{23,24} were fitted to the EGL model relying on transitions from a singly populated state (see Table II) and including transitions with $-8 \leq \Delta J \leq +10$ at most.

The population transfers based on the present EPGL fit compare well with those predicted using the EGL experimental model. As expected from the broadening coefficients predicted from the measurements of Frost²³ and Henton *et al.*²⁴ being smaller than the fit-

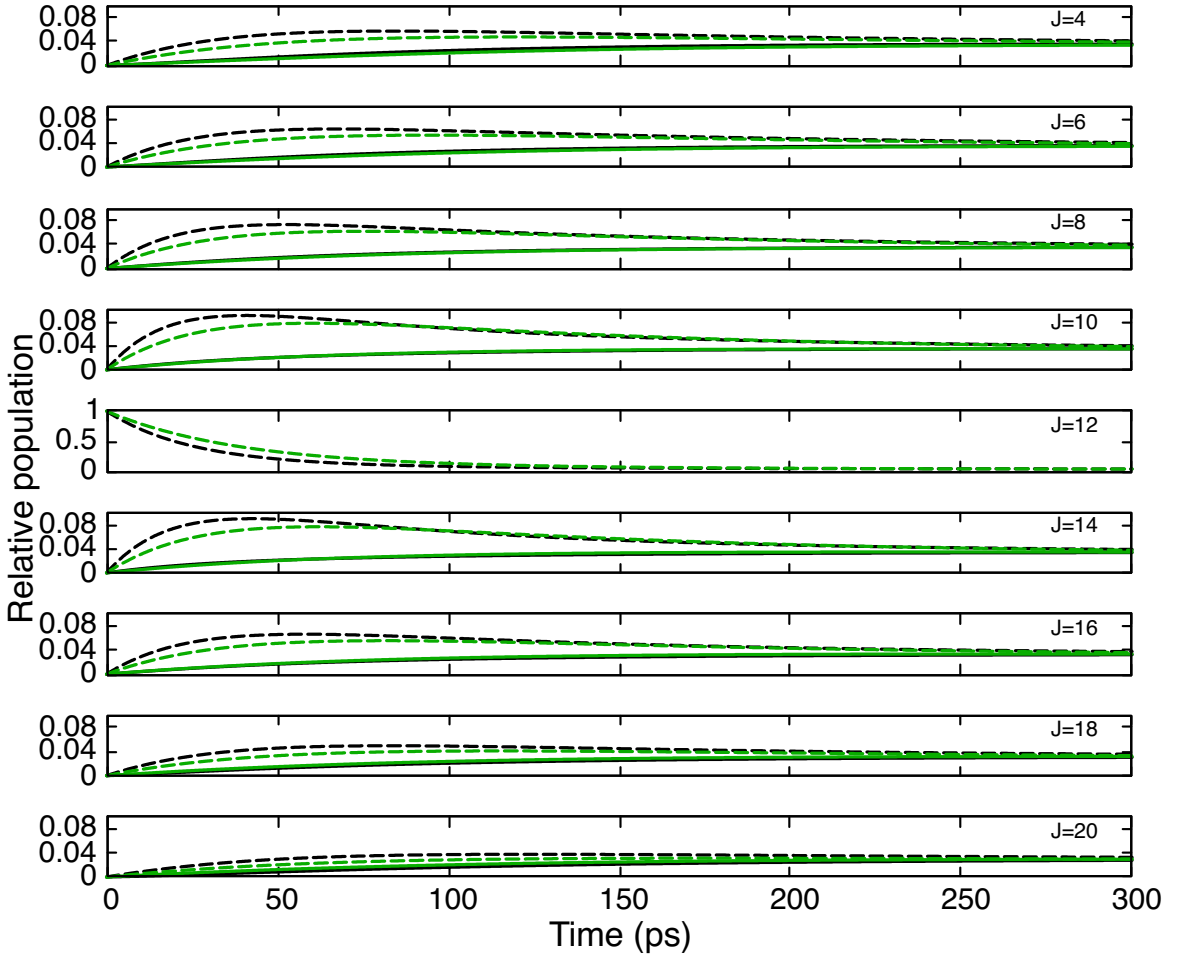


FIG. 3. Collision induced dynamics in Γ_1 (continuous) and in Γ_2 (dashed) from unitary population in the $|\Gamma_2, J = 12\rangle$ state under $P = 1$ atm. The state-to-state transition frequencies are calculated using the EPGL parameters listed in Table III (black) and the EGL experimental parameters reproduced in Table II (green).

ted broadening coefficients presented in Fig. 2, the transition frequencies calculated using the EPGL model are larger than the measured transitions frequencies.^{23,24} However, the dynamics happen on a similar timescale and the trends captured by the experiment are reproduced by the present model, *i.e.* the $|\Delta J| = 2$ propensity shown by the $J = 10$ and $J = 14$ curves that reflects the vicinity of levels energies and the faster fall of upwards transfers ($\Delta J > 0$) rather than the downwards transfers ($\Delta J < 0$).

In spite of the limitations mentioned here above, this methodology leads to good results given its simplicity, the number of parameters of the chosen fitting laws and the experimental

data used as the dynamics presented are very similar.

VI. CONCLUSIONS AND PERSPECTIVES

Two different methods allowing to extract the phenomenological parameters of the Lindblad equations from experimental data have been presented. In the first approach, the transitions frequencies are taken directly from a pump-probe experiment. In the second case, they are extracted from measured broadening coefficients. Both approaches rely on the use of the very simple Energy Gap laws and provide similar results with an unbeatable, inexpensive computational effort. Alternatively, the parameters could for example be calculated *ab-initio*. However, this would require the computation of an interaction potential, which can be very expensive due to the number of degrees of freedom, followed by the calculation of the S matrix.

The parameters obtained in this way allow to include rotational relaxation in dynamics simulations and in particular for laser control optimisations. We point out that the model being as good as its underlying approximations, it still depends strongly on assumptions. Main limitations follow that transient effects of collisions (non-Markovian effects⁴³) are not included limiting the validity to a finite range of frequencies⁴⁰ and Doppler broadening is neglected so that the model does not hold at low pressure.

In the case of the selected polyad of acetylene, we show that the rotational relaxation will induce a reorganisation of the populations initially confined in one J level in about 200 ps, which is very short to engage in a specific process. As stated before, the “dark” $|0101^{111}\rangle$ mode is not affected by the collisions on the same timescale due to selection rules. Indeed, parity-violation transitions should happen at the second to kilosecond timescale.³⁹ The $|0101^{111}\rangle$ mode can be seen as a “decoherence free” subspace, which makes it an interesting target for possible state-control studies.

ACKNOWLEDGMENTS

The authors warmly thank Michel Herman for very fruitful discussions. The IISN (Institut Interuniversitaire des Sciences Nucléaires) is acknowledged for its financial support. Computational resources have been provided by the Shared ICT Services Centre, Université

libre de Bruxelles.

DATA AVAILABILITY STATEMENT

The data that support the findings of this study are available from the corresponding author upon reasonable request.

REFERENCES

- ¹C. P. Koch, “Controlling open quantum systems: tools, achievements, and limitations,” *J. Phys. Condensed Mat.* **28**, 213001 (2016).
- ²C. P. Koch, M. Lemeshko, and D. Sugny, “Quantum control of molecular rotation,” *Rev. Mod. Phys.* **91**, 035005 (2019).
- ³B. Brüggemann, T. Pullerits, and V. May, “Laser pulse control of exciton dynamics in a biological chromophore complex,” *J. Photochem. Photobiol. A* **190**, 372–377 (2007).
- ⁴J. C. Tremblay and P. Saalfrank, “Guided locally optimal control of quantum dynamics in dissipative environments,” *Phys. Rev. A* **78**, 063408 (2008).
- ⁵J. C. Tremblay, S. Beyvers, and P. Saalfrank, “Selective excitation of coupled CO vibrations on a dissipative Cu (100) surface by shaped infrared laser pulses,” *J. Chem. Phys.* **128**, 194709 (2008).
- ⁶A. Chenel, G. Dive, C. Meier, and M. Desouter-Lecomte, “Control in a dissipative environment: The example of a Cope rearrangement,” *J. Phys. Chem. A* **116**, 11273–11282 (2012).
- ⁷L. Santos, N. Iacobellis, M. Herman, D. Perry, M. Desouter-Lecomte, and N. Vaeck, “A test of optimal laser impulsion for controlling population within the $N_s=1$, $N_r=5$ polyad of $^{12}\text{C}_2\text{H}_2$,” *Mol. Phys.* **113**, 4000–4006 (2015).
- ⁸L. Santos, M. Herman, M. Desouter-Lecomte, and N. Vaeck, “Rovibrational laser control targeting a dark state in acetylene. Simulation in the $N_s=1$, $N_r=5$ polyad,” *Mol. Phys.* **116**, 2213–2225 (2018).
- ⁹A. A. Michelson, “On the broadening of spectral lines,” *Astrophys. J.* **2**, 251 (1895).
- ¹⁰B. J. Orr and G. F. Nutt, “Rotationally resolved infrared-ultraviolet double resonance spectroscopy in molecular D_2CO and HDCO ,” *J. Mol. Spectrosc.* **84**, 272–287 (1980).

¹¹J. Karczmarek, J. Wright, P. Corkum, and M. Ivanov, “Optical centrifuge for molecules,” Phys. Rev. Lett. **82**, 3420 (1999).

¹²D. Villeneuve, S. Aseyev, P. Dietrich, M. Spanner, M. Y. Ivanov, and P. Corkum, “Forced molecular rotation in an optical centrifuge,” Phys. Rev. Lett. **85**, 542 (2000).

¹³R. Shafer and R. G. Gordon, “Quantum scattering theory of rotational relaxation and spectral line shapes in H₂–He gas mixtures,” J. Chem. Phys. **58**, 5422–5443 (1973).

¹⁴A. Lévy, N. Lacombe, and C. Chackerian Jr, “Collisional line mixing,” in *Spectroscopy of the Earth’s atmosphere and interstellar medium* (Academic Press Boston, 1992) pp. 261–337.

¹⁵J.-M. Hartmann, C. Boulet, and D. Robert, *Collisional Effects on Molecular Spectra: Laboratory Experiments and Models, Consequences for Applications* (Elsevier, 2008).

¹⁶J. Polanyi and K. Woodall, “Mechanism of rotational relaxation,” J. Chem. Phys. **56**, 1563–1572 (1972).

¹⁷T. A. Brunner and D. Pritchard, “Fitting laws for rotationally inelastic collisions,” in *Advances in Chemical Physics* (John Wiley & Sons, Ltd, 1982) pp. 589–641.

¹⁸C. Cousin, R. Le Doucen, C. Boulet, A. Henry, and D. Robert, “Line coupling in the temperature and frequency dependences of absorption in the microwindows of the 4.3 μ m CO₂ band,” J. Quant. Spectrosc. Radiat. Transf. **36**, 521–538 (1986).

¹⁹L. L. Strow and B. M. Gentry, “Rotational collisional narrowing in an infrared CO₂ Q branch studied with a tunable-diode laser,” J. Chem. Phys. **84**, 1149–1156 (1986).

²⁰B. M. Gentry and L. L. Strow, “Line mixing in a N₂-broadened CO₂ Q branch observed with a tunable diode laser,” J. Chem. Phys. **86**, 5722–5730 (1987).

²¹B. Amyay, A. Fayt, M. Herman, and J. Vander Auwera, “Vibration-rotation spectroscopic database on acetylene, $\tilde{X}^1\Sigma_g^+$ (¹²C₂H₂),” J. Phys. Chem. Ref. Data **45**, 023103 (2016).

²²J. Vander Auwera, D. Hurtmans, M. Carleer, and M. Herman, “The ν_3 Fundamental in C₂H₂,” J. Mol. Specrosc. **157**, 337–357 (1993).

²³M. J. Frost, “Energy Transfer in the 3₁, 2₁4₁5₁ Fermi-resonant States of acetylene. I. Rotational Energy Transfer,” J. Chem. Phys. **98**, 8572–8579 (1993).

²⁴S. Henton, M. Islam, S. Gatenby, and I. W. Smith, “Rotational Energy Transfer and Rotationally Specific Vibration–Vibration Intradyad Transfer in Collisions of C₂H₂ \tilde{X} $^1\Sigma_g^+$ (3₁/2₁4₁5₁, $J = 10$) with C₂H₂, Ar, He and H₂,” J. Chem. Soc. Far. Trans. **94**, 3219–3228 (1998).

²⁵P. R. Bunker, *Molecular symmetry and spectroscopy* (Academic Press, Inc., New York, 1979).

²⁶D. Jacquemart, J.-Y. Mandin, V. Dana, L. Régalia-Jarlot, X. Thomas, and P. Von der Heyden, “Multispectrum fitting measurements of line parameters for 5- μ m cold bands of acetylene,” *J. Quant. Spectrosc. Radiat. Transf.* **75**, 397–422 (2002).

²⁷J. Pliva, “Spectrum of acetylene in the 5-micron region,” *J. Mol. Spectrosc.* **44**, 145–164 (1972).

²⁸J. Pliva, “Molecular constants for the bending modes of acetylene $^{12}\text{C}_2\text{H}_2$,” *J. Mol. Spectrosc.* **44**, 165–182 (1972).

²⁹M. Herman, “The acetylene Ground State Saga,” *Mol. Phys.* **105**, 2217–2241 (2007).

³⁰G. Lindblad, “On the Generators of Quantum Dynamical Semigroups,” *Commun. Math. Phys.* **48**, 119–130 (1976).

³¹V. Gorini, A. Kossakowski, and E. C. G. Sudarshan, “Completely Positive Dynamical Semigroups of N-level Systems,” *J. Math. Phys.* **17**, 821–825 (1976).

³²T. Oka, “Collision-induced transitions between rotational levels,” in *Advances in atomic and molecular physics*, Vol. 9 (Elsevier, 1974) pp. 127–206.

³³M. Herman and J. Liévin, “Acetylene – From intensity alternation in spectra to ortho and para molecule,” *J. Chem. Educ.* **59**, 17 (1982).

³⁴A. P. Milce and B. J. Orr, “The $\nu_{\text{CC}}+3\nu_{\text{CH}}$ rovibrational manifold of acetylene. I. Collision-induced state-to-state transfer kinetics,” *J. Chem. Phys.* **106**, 3592–3606 (1997).

³⁵H. Rabitz, “Rotation and rotation-vibration pressure-broadened spectral lineshapes,” *Annu. Rev. Phys. Chem.* **25**, 155–177 (1974).

³⁶R. G. Gordon, “Semiclassical theory of spectra and relaxation in molecular gases,” *J. Chem. Phys.* **45**, 1649–1655 (1966).

³⁷C. J. Meinrenken, W. D. Gillespie, S. Macheret, W. R. Lempert, and R. B. Miles, “Time domain modeling of spectral collapse in high density molecular gases,” *J. Chem. Phys.* **106**, 8299–8309 (1997).

³⁸D. Manzano, “A short introduction to the Lindblad Master Equation,” *AIP Adv* **10**, 025106 (2020).

³⁹M. Herman, “High-resolution infrared spectroscopy of acetylene: theoretical background and research trends,” in *Handbook of High-Resolution Spectroscopy*, edited by M. Quack and F. Merkt (John Wiley & Sons, Ltd., 2011).

⁴⁰A. Ben-Reuven, “Impact broadening of microwave spectra,” Phys. Rev. **145**, 7 (1966).

⁴¹B. Amyay, A. Fayt, and M. Herman, “Accurate partition function for acetylene, $^{12}\text{C}_2\text{H}_2$, and related thermodynamical quantities,” J. Chem. Phys. **135**, 234305 (2011).

⁴²A. Pine, “Self-, N_2 -and Ar-broadening and line mixing in HCN and C_2H_2 ,” J. Quant. Spectrosc. Radiat. Transf. **50**, 149–166 (1993).

⁴³U. Fano, “Pressure broadening as a prototype of relaxation,” Phys. Rev. **131**, 259 (1963).

⁴⁴D. Jacquemart, J.-Y. Mandin, V. Dana, L. Régalia-Jarlot, J.-J. Plateaux, D. Décatoire, and L. Rothman, “The spectrum of acetylene in the 5- μm region from new line-parameter measurements,” J. Quant. Spectrosc. Radiat. Transf. **76**, 237–267 (2003).

⁴⁵I. E. Gordon, L. S. Rothman, C. Hill, R. V. Kochanov, Y. Tan, P. F. Bernath, M. Birk, V. Boudon, A. Campargue, K. Chance, *et al.*, “The HITRAN2016 molecular spectroscopic database,” J. Quant. Spectrosc. Radiat. Transf. **203**, 3–69 (2017).

⁴⁶B. Orr, “Collision-Induced State-to-State Energy Transfer in Perturbed Rovibrational Manifolds of Small Polyatomic Molecules: Mechanistic Insights and Observations,” Chem. Phys. **190**, 261–278 (1995).

⁴⁷S. Henton, M. Islam, and I. W. Smith, “Relaxation within and from the $(3_1/2_14_15_1)$ and $(3_14_1/2_14_25_1)$ Fermi Dyads in acetylene: Vibrational Energy Transfer in Collisions with C_2H_2 , N_2 and H_2 ,” J. Chem. Soc., Far. Trans. **94**, 3207–3217 (1998).

⁴⁸E. Jones, T. Oliphant, P. Peterson, *et al.*, “SciPy: Open source scientific tools for Python,” (2001–).

Supplemental Material: Lindblad parameters from high resolution spectroscopy to describe collision induced decoherence in the gas phase - Application to acetylene

S1. LINDBLAD MASTER EQUATION IMPLEMENTATION

We develop here the second term of the Lindblad master equation:

$$\begin{aligned} \frac{d\hat{\rho}(t)}{dt} &= -\frac{i}{\hbar} [\hat{H}(t), \hat{\rho}(t)] + \hat{\mathcal{L}}_D \hat{\rho}(t) \\ &= -\frac{i}{\hbar} [\hat{H}(t), \hat{\rho}(t)] + \sum_{jk} \left(\hat{L}_{jk} \hat{\rho}(t) \hat{L}_{jk}^\dagger - \frac{1}{2} [\hat{\rho}(t), \hat{L}_{jk}^\dagger \hat{L}_{jk}]_+ \right) \end{aligned} \quad (\text{S1})$$

with $\hat{H}(t)$ the total hamiltonian in absence of interaction with the environment, $\hat{\rho}$ the density operator, \hat{L}_{jk} are transitions operators between states j and k and $[A, B]_+$ is the anti-commutator of arguments A and B . A phenomenological representation of the transition operator is used, with θ_{jk} the transmission frequencies² between the system hamiltonian eigenstates $\{|j\rangle\}$:

$$\hat{L}_{jk} = \sqrt{\theta_{jk}} |j\rangle \langle k|. \quad (\text{S2})$$

Development of Eq. S1 is given below:

$$\begin{aligned} \hat{\mathcal{L}}_D \hat{\rho}(t) &= \sum_{jk} \left(\hat{L}_{jk} \hat{\rho}(t) \hat{L}_{jk}^\dagger - \frac{1}{2} [\hat{\rho}(t), \hat{L}_{jk}^\dagger \hat{L}_{jk}]_+ \right) \\ &= \sum_{jk} \sqrt{\theta_{jk}} |j\rangle \langle k| \hat{\rho}(t) \sqrt{\theta_{kj}} |k\rangle \langle j| \\ &\quad - \frac{1}{2} \left[\hat{\rho}(t) \sqrt{\theta_{kj}} |k\rangle \langle j| \sqrt{\theta_{jk}} |j\rangle \langle k| + \sqrt{\theta_{kj}} |k\rangle \langle j| \sqrt{\theta_{jk}} |j\rangle \langle k| \hat{\rho}(t) \right] \end{aligned}$$

θ_{jk} et θ_{kj} are scalars and not necessarily equal;

$$\begin{aligned} \hat{\mathcal{L}}_D \hat{\rho}(t) &= \sum_{jk} \sqrt{\theta_{jk}} \sqrt{\theta_{kj}} |j\rangle \langle k| \hat{\rho}(t) |k\rangle \langle j| - \frac{1}{2} \sqrt{\theta_{jk}} \sqrt{\theta_{kj}} [\hat{\rho}(t) |k\rangle \langle j| \langle j| \langle k| + |k\rangle \langle j| \langle j| \langle k| \hat{\rho}(t)] \\ &= \sum_{jk} \sqrt{\theta_{jk}} \sqrt{\theta_{kj}} |j\rangle \langle k| \hat{\rho}(t) |k\rangle \langle j| - \frac{1}{2} \sqrt{\theta_{jk}} \sqrt{\theta_{kj}} [\hat{\rho}(t) |k\rangle \langle k| + |k\rangle \langle k| \hat{\rho}(t)] \end{aligned}$$

The diagonal elements are given by:

$$\begin{aligned} \langle n | \hat{\mathcal{L}}_D \hat{\rho}(t) | n \rangle &= \sum_{jk} \left(\sqrt{\theta_{jk}} \sqrt{\theta_{kj}} \langle n | j \rangle \langle k | \hat{\rho}(t) | k \rangle \langle j | n \rangle \right. \\ &\quad \left. - \frac{1}{2} \sqrt{\theta_{jk}} \sqrt{\theta_{kj}} [\langle n | \hat{\rho}(t) | k \rangle \langle k | n \rangle + \langle n | k \rangle \langle k | \hat{\rho}(t) | n \rangle] \right) \end{aligned}$$

² The use of θ is a deliberate choice, literature generally uses γ .

The first terms is non-zero if and only if $\langle n|j\rangle \neq 0$, *i.e.*, if $j = n$. In the second term, $\langle n|k\rangle \neq 0$ only if $n = k$. The sum over j disappears in the first term and over k in the second term.

$$\begin{aligned}\langle n|\hat{\mathcal{L}}_D\hat{\rho}(t)|n\rangle &= \sum_k \sqrt{\theta_{nk}}\sqrt{\theta_{kn}}\rho_{kk}(t) - \sum_j \frac{1}{2} \left[\sqrt{\theta_{jn}}\sqrt{\theta_{nj}}\rho_{nn}(t) + \sqrt{\theta_{jn}}\sqrt{\theta_{nj}}\rho_{nn}(t) \right] \\ &= \sum_k \sqrt{\theta_{nk}}\sqrt{\theta_{kn}}\rho_{kk}(t) - \sum_j \sqrt{\theta_{jn}}\sqrt{\theta_{nj}}\rho_{nn}(t)\end{aligned}\quad (\text{S3})$$

The non-diagonal elements are given by:

$$\begin{aligned}\langle n|\hat{\mathcal{L}}_D\hat{\rho}(t)|m\rangle &= \sum_{jk} \left(\sqrt{\theta_{jk}}\sqrt{\theta_{kj}}\langle n|j\rangle\langle k|\hat{\rho}(t)|k\rangle\langle j|m\rangle \right. \\ &\quad \left. - \frac{1}{2}\sqrt{\theta_{jk}}\sqrt{\theta_{kj}} [\langle n|\hat{\rho}(t)|k\rangle\langle k|m\rangle + \langle n|k\rangle\langle k|\hat{\rho}(t)|m\rangle] \right)\end{aligned}$$

The first term is always zero ($n \neq m$) and the second term is non-zero if $k = m$,

$$\begin{aligned}\langle n|\hat{\mathcal{L}}_D\hat{\rho}(t)|m\rangle &= -\frac{1}{2} \left[\sum_j \sqrt{\theta_{jm}}\sqrt{\theta_{mj}}\rho_{nm}(t) + \sqrt{\theta_{jn}}\sqrt{\theta_{nj}}\rho_{nm}(t) \right] \\ &= -\frac{1}{2}\rho_{nm}(t) \sum_j \left(\sqrt{\theta_{jm}}\sqrt{\theta_{mj}} + \sqrt{\theta_{jn}}\sqrt{\theta_{nj}} \right)\end{aligned}\quad (\text{S4})$$

S2. SIMULATION OF SPECTRA USING THE RELAXATION MATRIX

Absorption spectra, *i.e.* the absorption coefficient as a function of the wavenumber, can be calculated using Eq. 5 of the main text. All the parameters involved are self-explanatory or identified there. However, the calculation of the equilibrium relative population ρ_ℓ in the ground vibrational state of acetylene associated with line ℓ is worth an explanation. Separate relative equilibrium populations are calculated for ortho (J odd) and para (J even) $^{12}\text{C}_2\text{H}_2$.³³ They are given by³⁹

$$\rho_{J_{\text{ortho}}} = \frac{\exp [-(E_{J_{\text{ortho}}} - E_{J=1}) / k_B T]}{\sum_{J_{\text{ortho}}} \exp [-(E_{J_{\text{ortho}}} - E_{J=1}) / k_B T]} \quad (\text{S5})$$

$$\rho_{J_{\text{para}}} = \frac{\exp [-(E_{J_{\text{para}}} - E_{J=0}) / k_B T]}{\sum_{J_{\text{para}}} \exp [-(E_{J_{\text{para}}} - E_{J=0}) / k_B T]} \quad (\text{S6})$$

with k_B the Boltzmann constant, and T the temperature. The distributions of ortho- and para-acetylene, centered at $J = 9$ are illustrated in Fig. S1.

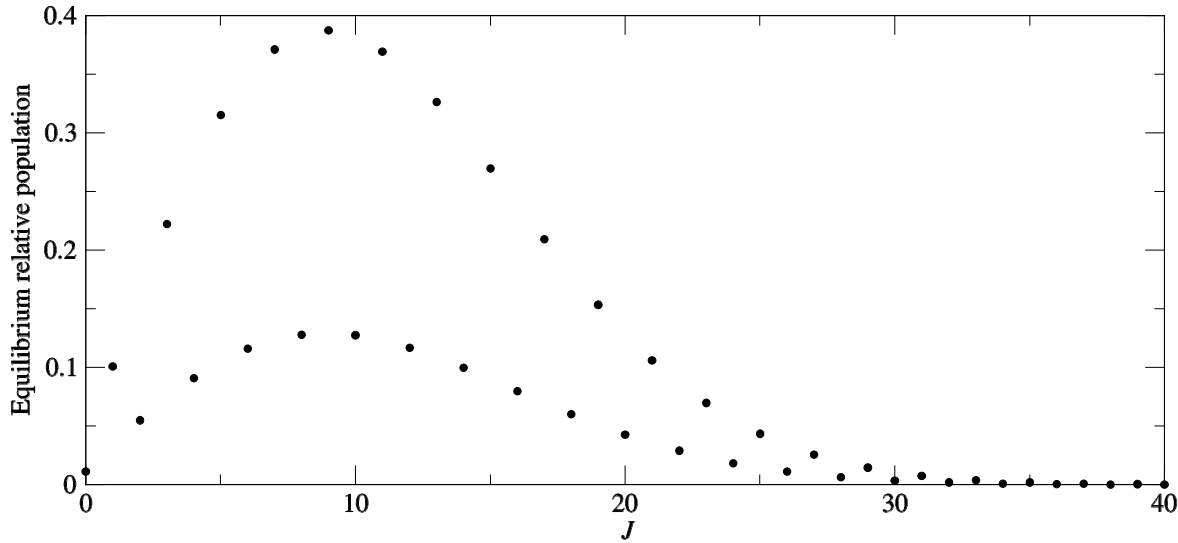


FIG. S1. Boltzmann population distribution of ortho- and para-acetylene in its ground vibrational state at $T = 296$ K, normalized so that the sum of all the values is equal to 4.

As an argument supporting the validity of the broadening coefficients calculated using the EGL parameters determined in this work (listed in Table III), the absorption spectrum of the ν_3 band of $^{12}\text{C}_2\text{H}_2$ at 1 atm and 296 K was calculated two ways. The black trace in Fig. S2 was obtained using Eq. 5 with only the real part of the diagonal elements

of the relaxation matrix W being non zero, therefore ignoring line shifts and line mixing. The broadening coefficients of R and P branch lines were calculated as described in the main text using the EGL parameters of Table III. The red trace displays the differences between the same spectrum calculated using a sum of Lorentzian lines with the parameters available in the HITRAN database⁴⁵ and the black trace. Note that the black spectrum was actually calculated using line positions from the effective Hamiltonian of Amyay *et al.*²¹ and transition dipole moments from Vander Auwera *et al.*²² However, the differences with the line positions and intensities available in HITRAN are only marginal, with a root mean square deviation of 0.0007 cm^{-1} . Fig. S2 shows that, although the EGL model does not fit perfectly the experimental broadening coefficients²⁶ (see Fig. 2), the differences are at most 10%.

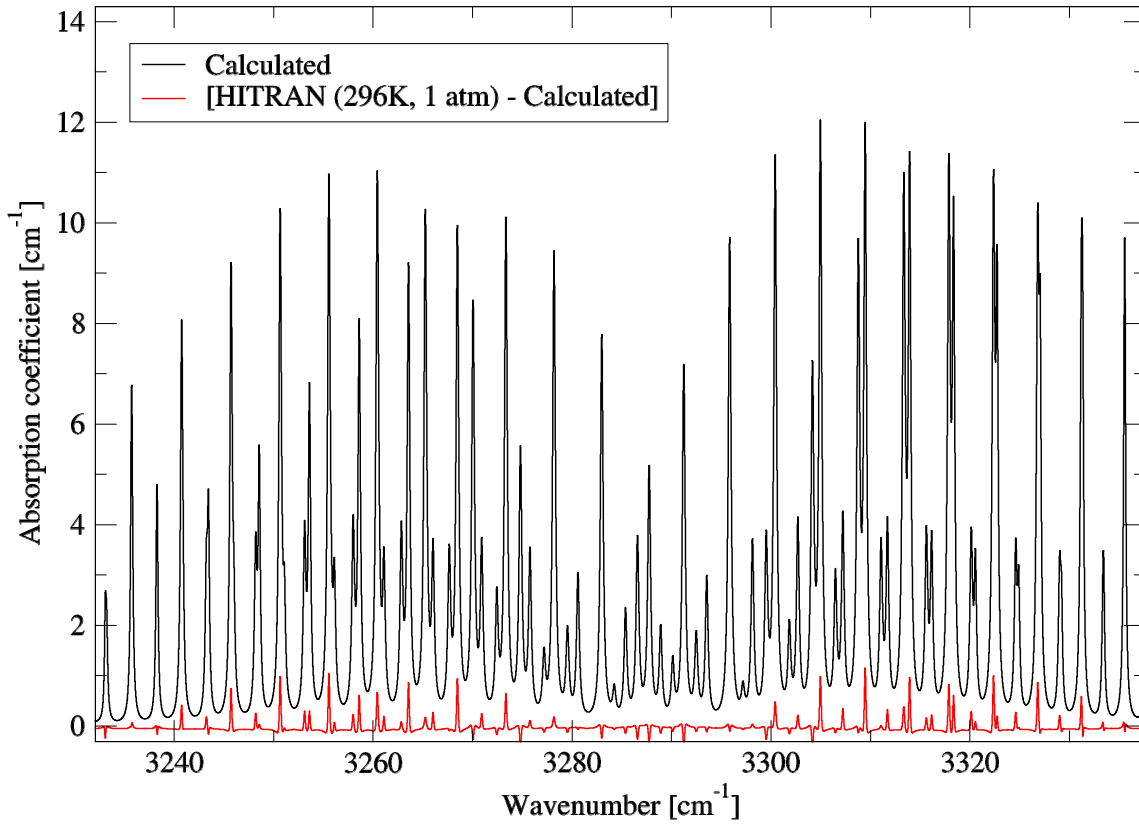


FIG. S2. Calculated spectrum of the ν_3 band of $^{12}\text{C}_2\text{H}_2$ at $P = 1 \text{ atm}$ and $T = 296 \text{ K}$.